Advances in Water Resources 34 (2011) 1249–1255

Contents lists available at ScienceDirect

Advances in Water Resources

journal homepage: www.elsevier.com/locate/advwatres

Monodisperse and polydisperse colloid transport in water-saturated fractures with various orientations: Gravity effects

Scott C. James [a,*], Constantinos V. Chrysikopoulos [b]

[a] Sandia National Laboratories, Thermal/Fluid Science & Engineering, P.O. Box 969, Livermore, CA 94551-0969, USA
[b] Department of Civil Engineering, University of Patras, Patras 26500, Greece

ARTICLE INFO

Article history:
Received 16 March 2011
Received in revised form 31 May 2011
Accepted 2 June 2011
Available online 17 June 2011

Keywords:
Colloid transport
Particle tracking
Fracture flow and transport
Gravitational effects
Dense colloids
Polydisperse colloid suspensions

ABSTRACT

Numerical experiments are conducted to examine the effects of gravity on monodisperse and polydisperse colloid transport in water-saturated fractures with uniform aperture. Dense colloids travel in water-saturated fractures by advection and diffusion while subject to the influence of gravity. Colloids are assumed to neither attach onto the fracture walls nor penetrate the rock matrix based on the assumptions that they are inert and their size is larger than the pore size of the surrounding solid matrix. Both the size distribution of a colloid plume and colloid density are shown to be significant factors impacting their transport when gravitational forces are important. A constant-spatial-step particle-tracking code simulates colloid plumes with increasing densities transporting in water-saturated fractures while accounting for three forces acting on each particle: a deterministic advective force due to the Poiseuille flow field within the fracture, a random force caused by Brownian diffusion, and the gravitational force. Integer angles of fracture orientation with respect to the horizontal ranging from ±90° are considered: three lognormally distributed colloid plumes with mean particle size of 1 μm (averaged on a volumetric basis) and standard deviation of 0.6, 1.2 and 1.8 μm are examined. Colloid plumes are assigned densities of 1.25, 1.5, 1.75 and 2.0 g/cm^3. The first four spatial moments and the first two temporal moments are estimated as functions of fracture orientation angle and colloid density. Several snapshots of colloid plumes in fractures of different orientations are presented. In all cases, larger particles tend to spread over wider sections of the fracture in the flow direction, but smaller particles can travel faster or slower than larger particles depending on fracture orientation angle.

1. Introduction

In fractured subsurface formations, colloids are either produced by microerosion of rock minerals as a result of formation crushing due to tectonic activity, chemical dissolution of rock minerals caused by water infiltration, and changes in groundwater geochemical conditions [1,2, p. 93] or they are introduced during artificial recharge of reclaimed wastewater [3,4]. Groundwater contaminants often exhibit higher affinity for attachment onto colloids than onto formation solid surfaces [5]. Consequently, colloids often serve as carriers for contaminants and may significantly influence the net rate of contaminant migration in subsurface formations [6–8].

Most of the published mathematical models for colloid transport or contaminant/colloid cotransport in fractured systems assume that colloids are of uniform size (monodisperse colloid suspensions) [5,9–11]. Colloids present in groundwaters frequently follow a lognormal distribution in diameter [12]. However, just a few studies for colloid transport in fractures based on particle tracking simulations have examined the realistic case of variably sized colloid (polydisperse colloid suspensions) transport in water saturated fractures, accounting for both matrix diffusion and colloid deposition [13,14].

This work focuses on the transport of dense monodisperse and polydisperse colloid plumes in a fracture with uniform aperture. The effects of gravity, fracture orientation, and polydispersity on colloid transport are investigated.

2. Mathematical development

2.1. Fracture

Consider a two-dimensional, water saturated fracture with length $x = 8$ m that is rotated through 180° to capture the effects on polydisperse colloid transport from gravity (see Fig. 1). Water movement is from bottom to top in that orientation. No-flow boundary conditions are imposed along the fracture walls. Flow in the rock matrix is neglected because the saturated hydraulic conductivity in the rock matrix is several orders of magnitude

* Corresponding author.
E-mail address: scjames@sandia.gov (S.C. James).

0309-1708/$ - see front matter © 2011 Elsevier Ltd. All rights reserved.
doi:10.1016/j.advwatres.2011.06.001

Nomenclature

d_p	colloid particle diameter, L
D	molecular diffusion coefficient, L^2/t
g	gravitational acceleration, L^2/t
k_B	Boltzmann's constant; 1.381×10^{-23} J/K, $(M L^2)/(t^2 T)$
m	spatial step number (–)
$m_n(x)$	nth absolute temporal moment, t^n
$M_n(x)$	nth normalized temporal moment, t^n
$\overline{M}_n(t)$	nth normalized spatial moment, L^n
n	order of moment (–)
N	colloid number concentration (1/L in 1D)
N_p	number of colloid particles (–)
N_{p_0}	total number of colloid particles (–)
t	time, t
T	temperature, T
U	interstitial flow velocity, L/t
$\overline{U}$	mean interstitial flow velocity, L/t
U_s	colloid particle terminal velocity, L/t
x	spatial location perpendicular to gravity, L
z	spatial location in the direction of gravity, L
$Z(0,1)$	random selection from the standard normal distribution (–)

Greek letters

η	fluid dynamic viscosity, M/(L t)
μ	volume-averaged mean colloid diameter, L
$\mu_n(t)$	nth absolute spatial moment, L^n
ρ_f	fluid density, M/L^3
ρ_p	colloid particle density, M/L^3
σ	standard deviation, L
σ^2	variance, L^2
ω	time-step number (–)
Ω_1	empirical constant (–)
Ω_2	empirical constant (–)

smaller than the saturated hydraulic conductivity within the fracture [15]. Colloids are introduced in proportion to the local flow rate at the upstream inlet and it is assumed that they neither deposit onto the fracture surfaces nor penetrate the solid matrix.

2.2. Modeling of colloid transport by particle tracking

Numerous published studies focus on modeling colloid transport in fractures and use various analytical and numerical solution techniques for the governing partial differential equations. Analytical solutions are applied to simple physicochemical conditions and fracture geometries [16–20], more complex situations require finite element or finite difference approximations that suffer from numerical dispersion [5,7–9,21,22], and other investigations employ particle tracking techniques that may require significant computational power [11,13,14,23–28]. In this study, colloid transport is simulated with particle tracking.

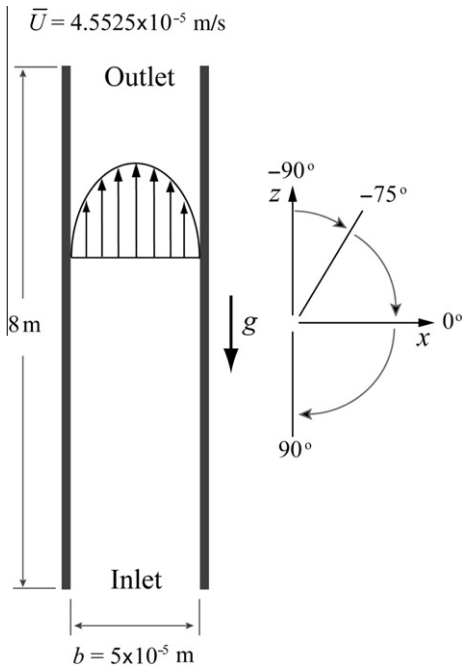

Fig. 1. Schematic illustration of the fracture and its orientations with respect to gravity.

Particle tracking is the simplest method that can account for both variably sized (polydisperse) colloids and irregular boundaries (spatially variable aperture), because a unique set of parameters is allocated to each particle to store its permanent and continuously changing characteristics (e.g., location, size, sorption status, and gravitational properties). Furthermore, particle tracking procedures provide stochastic solutions to linear partial differential equations that do not suffer from numerical dispersion [29]. Traditional particle-tracking equations for colloid transport in water-saturated fractures update spatial locations over a constant time step. They consist of two terms: a deterministic term representing advection processes, and a stochastic term simulating random molecular diffusion. However, traditional particle-tracking equations with a constant time step may be inappropriate for polydisperse colloids, because during the pre-determined time step, a small particle will experience a significantly greater diffusional effect than a large particle. By specifying *a priori* a spatial step for transport across streamlines and determining the random time required by each particle to travel this distance, the movement of small and large colloids is modeled with equal accuracy. In this work, constant-spatial-step (continuous time random walk) particle-tracking equations are used [30,31].

2.3. Transport of neutrally buoyant colloids

For neutrally buoyant polydisperse colloid plumes, each particle is transported through the water-saturated fracture according to the following equations:

$$x_m = x_{m-1} + U(x_{m-1}, z_{m-1})\Delta t + Z(0,1)\sqrt{2D\Delta t}, \quad (1)$$

$$z_m = z_{m-1} \pm \Delta z, \quad (2)$$

where $U(x,z)$ is a Poiseuille velocity profile, $Z(0,1)$ is a random selection from the standard normal distribution, m is the spatial step number, and D is the molecular diffusion coefficient specified for a spherical particle by the Stokes–Einstein diffusion equation [32]:

$$D = \frac{k_B T}{3\pi\eta d_p}, \quad (3)$$

where d_p is the particle diameter, k_B is Boltzmann's constant, η is the fluid dynamic viscosity, and T is the temperature of the interstitial fluid. The direction of the displacement $\pm\Delta z$ in (2) is determined from the sign of another standard normally distributed random number, $Z(0,1)$. The time step, Δt, employed in (1) is [30]:

$$\Delta t = \exp\left\{\ln\left[\frac{(\Delta z)^2}{D}\right] - \Omega_1 + \Omega_2 \cdot Z(0,1)\right\}, \quad (4)$$

$$\Omega_1 = 0.979 \pm 0.012, \quad (5)$$

$$\Omega_2 = 0.787 \pm 0.002. \quad (6)$$

Eqs. (4)–(6) represent a random selection of Δt from the lognormal distribution of the travel times for a particle with molecular diffusion coefficient D traveling a distance Δz. Following the selection of an appropriate value for Δz and substitution of (3) into (4), a random time step Δt is calculated and used in (1). It should be noted that for traditional particle tracking with a constant time step, (2) should be replaced by

$$z_m = z_{m-1} + Z(0,1)\sqrt{2D\Delta t}. \quad (7)$$

For the present study, the fracture walls are considered impermeable to colloids. Consequently, it is assumed that when particles encounter fracture walls they are reflected back as in a mirror image without loss of energy. That is, for a horizontal orientation or zero fracture angle, the final x coordinate remain unchanged, whereas the final z coordinate is set a distance away from the wall equal to the distance that the particle would have obtained if it had penetrated the rock matrix plus the particle diameter. For example, if a particle of $d_p = 1 \times 10^{-6}$ m is initially estimated to move to a z location of 5.03×10^{-5} m (5.0×10^{-5} m being the location of the fracture wall), its reflected z location would be 4.87×10^{-5} m. Also, it should be noted that the center of a colloid particle cannot reach the location $z = 0$ due to its finite size. Therefore, near the fracture wall, a colloid may move by diffusion as well as advection because its velocity component, U_x, although small, is never equal to zero.

2.4. Transport of dense colloids

For polydisperse colloid plumes subject to gravitational forces, the effects of gravitational settling on each colloid must be incorporated into the particle tracking equations. Assuming that a colloid is reasonably represented by a small sphere, for a density difference between the colloid and the suspending fluid, the balance among gravity, buoyancy, and viscous forces yields a terminal settling velocity of [32, p. 395]

$$U_s = -\frac{(\rho_p - \rho_f) g d_p^2}{18\eta}, \quad (8)$$

where ρ_f and ρ_p are the densities of the suspending fluid and the colloid particle, respectively, and g is the acceleration due to gravity in the negative z direction (although it has a component along or against the flow direction when the fracture is non-vertical).

The transport of colloids in the x direction is not affected by gravitational settling. Consequently, the appropriate particle tracking equations for dense colloids are (1) and

$$z_m = z_{m-1} \pm \Delta z + U_s \Delta t, \quad (9)$$

where the direction of the displacement, $\pm\Delta z$, is determined again from the sign of a standard normally distributed random number, $Z(0,1)$. Selecting an appropriate value for Δz and substituting (3) into (4), a random time step Δt is calculated for use in (1) and (9).

2.5. Colloid plumes

One monodisperse and three polydisperse colloid plumes are selected for the model simulations. Each plume consists of a total number of $N_0 = 10{,}000$ colloids, a number that yields appropriately low random noise. The larger the number of particles, the smaller the contribution of each particle to the overall transport behavior of a colloid plume, and thus the smoother the results. All colloid suspensions have the same volume-averaged mean colloid diameter, $\mu_{d_p} = 1$ μm. However, the three polydisperse colloid suspensions with standard deviation of colloid diameters $\sigma_{d_p} = 0.6$, 1.2, and 1.8 μm, respectively, are assumed to follow a lognormal size distribution [33]

$$N_p(d_p) = \frac{N_{p0}}{(2\pi)^{1/2}\sigma_{\ln d_p} d_p} \exp\left[-\frac{1}{2}\left(\frac{\ln d_p - \mu_{\ln d_p}}{\sigma_{\ln d_p}}\right)^2\right], \quad (10)$$

where $N_p(d_p)$ is the number of colloids with a given diameter d_p, $\mu_{\ln d_p}$ is the mean log-transformed colloid diameter, and $\sigma^2_{\ln d_p}$ is the variance of the log-transformed colloid diameter distribution. Note that the mean colloid diameter is represented by

$$\mu_{d_p} = \exp(\mu_{\ln d_p} + 0.5\sigma^2_{\ln d_p}) \quad (11)$$

and the variance of the colloid diameter distribution by

$$\sigma^2_{d_p} = \mu^2_{d_p}\left[\exp\left(\sigma^2_{\ln d_p}\right) - 1\right]. \quad (12)$$

The size distributions of each plume are shown in Fig. 2. The colloid densities considered in this study are $\rho_p = 1.25$, 1.50, 1.75, and 2.0 g/cm^3, whereas the density of water is assumed to be $\rho_f = 1.0$ g/cm^3.

Values for $\mu_{\ln d_p}$ and $\sigma^2_{\ln d_p}$ were calculated from (11) and (12) using $\mu_{d_p} = 1$ μm and $\sigma_{d_p} = 0.6$, 1.2, and 1.8 μm and these substituted into (10). Discrete colloid sizes were incremented in units of 0.01 μm and N_{p_0} was selected such that $\Sigma N_p(d_p) = 10{,}000$. Colloids are distributed at the fracture inlet according to the volumetric flow rate as suggested by Reimus [23]. The probability of a colloid entering at a given z location (perpendicular to the fracture walls) is proportional to the flow rate

$$P(z) = -2\left(\frac{z}{b}\right)^2 + \frac{3}{2}\frac{z}{b} + \frac{1}{2}. \quad (13)$$

A uniform random number between zero and one is substituted for $P(z)$ in the preceding equation and the roots calculated. Roots found outside of the range of $\pm b/2$ are discarded and colloids must be wholly contained within the fracture (adding the colloid's radius to the centroid calculation of (13) must not overlap with the fracture wall).

2.6. Moments

2.6.1. Temporal moments

In this study, the colloid concentration breakthrough distributions obtained at location $x = L$ are analyzed by the absolute temporal moments, which are defined as:

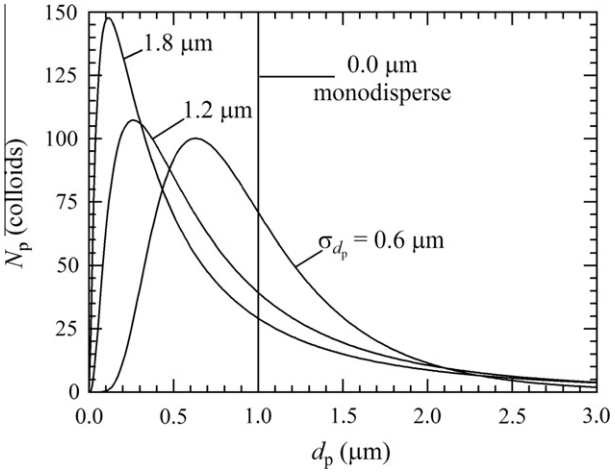

Fig. 2. Lognormal size distributions of the colloid plumes.

$$m_n(x) = \int_0^\infty t^n N(x,t)\mathrm{d}t, \tag{14}$$

where N is the colloid number concentration and the subscript $n = 0,1,2,\ldots$ indicates the order of the moment. The zeroth absolute temporal moment, m_0, quantifies the total mass in the breakthrough distribution of suspended colloids; the first absolute moment, m_1, describes the mean residence time of suspended colloids; and the second absolute moment, m_2, describes the degree of spreading of the suspended colloid breakthrough distribution. For the present study, the zeroth absolute temporal moment equals the total number of particles divided by the mean flow velocity ($m_0 = N_{p_0}\overline{U}$) because we have assumed that colloids neither deposit onto the fracture walls nor penetrate the solid matrix. In addition to the absolute moments, the normalized temporal moments are often employed, which are defined as:

$$M_n(x) = \frac{m_n(x)}{m_0(x)} = \frac{\int_0^\infty t^n N(x,t)\mathrm{d}t}{\int_0^\infty N(x,t)\mathrm{d}t}. \tag{15}$$

The first normalized temporal moment, M_1, defines the mean breakthrough time (residence time), or average velocity. The second normalized temporal moment, M_2, characterizes the temporal spreading of the suspended colloid breakthrough distribution (variance of residence-time distribution). One frequently employed method for normalized temporal-moment estimation of experimental or distinct data applies the unbiased trapezoidal integration scheme as follows [34]:

Table 1
Model and system parameters.

Parameter	Symbol	Value(s)
Fracture aperture	b	5×10^{-5} m
Average flow velocity	$\overline{U}$	4.5525×10^{-5} m/s
Water temperature	T	20 °C
Water viscosity	η	10^{-3} N s/m^2
Water density	ρ_f	10^3 kg/m^3
Average colloid diameter	μ	10^{-6} m
Colloid standard deviation	σ	0.6, 1.2, 1.8×10^{-6} m
Colloid densities	ρ_p	1.25, 1.5, 1.75, 2×10^3 kg/m^3

$$M_n(x) = \frac{\sum_{i=2}^{\omega} \frac{1}{2}\left(t_i^n N_i + t_{i-1}^n N_{i-1}\right)(t_i - t_{i-1})}{\sum_{i=2}^{\omega} \frac{1}{2}(N_i + N_{i-1})(t_i - t_{i-1})} = \frac{1}{N_{p_0}} \sum_{i=2}^{\omega} \left(\frac{t_i^n N_i + t_{i-1}^n N_{i-1}}{2}\right)(t_i - t_{i-1}), \tag{16}$$

where $N_i = N(x,t_i)$ is the colloid particle number concentration at time $t = t_i$, and ω is the number of time steps.

2.6.2. Spatial moments

Spatial moment analysis was introduced by Aris [35] and since then it has been applied to numerous solute transport studies [36–40]. In this study, the distributions of suspended colloids within the fracture (snapshots) are analyzed by the absolute spatial moments, which are defined as:

$$\mu_n(t) = \int_0^\infty x^n N(x,t)\mathrm{d}x, \tag{17}$$

where the subscript $n = 0,1,2,\ldots$ indicates the order of the moment. The zeroth absolute spatial moment, μ_0, quantifies the total mass in the suspended colloid distribution; the first absolute moment, μ_1, describes the center of mass of the suspended colloids; and second absolute moment, μ_2, describes the degree of spreading of the suspended colloids. For the present study (colloids neither deposit onto the fracture walls nor penetrate into the solid matrix), the zeroth absolute spatial moment equals the total number of particles ($\mu_0 = N_0$). In addition to the absolute spatial moments, the normalized spatial moments are often employed, which are defined as:

$$\overline{M}_n(t) = \frac{\mu_n(t)}{\mu_0(t)} = \frac{\int_0^\infty x^n N(x,t)\mathrm{d}x}{\int_0^\infty N(x,t)\mathrm{d}x}. \tag{18}$$

The normalized spatial moments of experimental or distinct data are estimated by:

$$\overline{M}_n(t) = \frac{1}{N_{p0}} \sum_{i=2}^{\omega} \left[\frac{(x_i + x_{i-1})}{2} - \overline{M}_1(t)\right]^n \left(\frac{N_i + N_{i-1}}{2}\right)(x_i - x_{i-1}). \tag{19}$$

Note that $\overline{M}_1$ as evaluated by (19) represents the center of mass for a monodisperse plume, but is not necessarily so for polydisperse plumes.

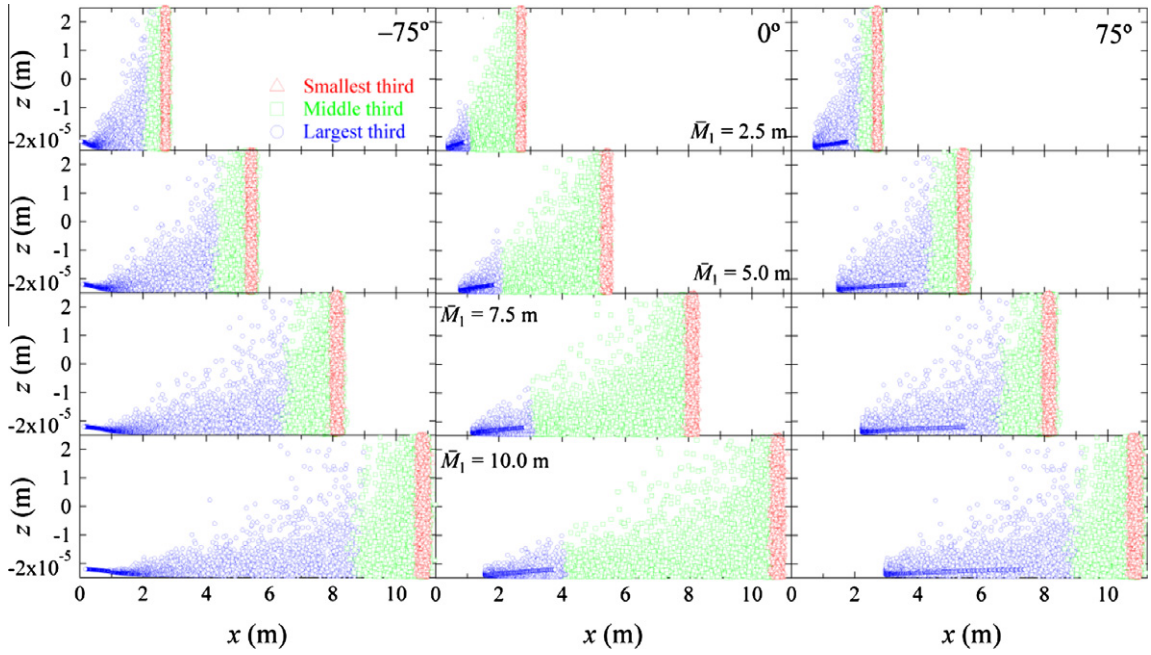

Fig. 3. Snapshots of polydisperse particle plume ($\sigma_{d_p} = 1.2$ μm) with colloid densities of 1.75 g/cm^3 at fracture angles of −75°, 0°, and 75° from left to right.

3. Model simulations

Model simulations for the transport of dense polydisperse colloids in a uniform-aperture fracture are performed for 181 different representations of gravity with limits shown in Fig. 1 (unit angle increments from −90° to 90°). The fracture aperture is specified as $b = 5 \times 10^{-5}$ m and the mean flow velocity is $\overline{U} = 4.5525 \times 10^{-5}$ m/s, which means that it takes water nearly 49 h to traverse the 8-m fracture. Water at 20 °C has a viscosity of approximately 10^{-3} N s/m^2. Table 1 lists the colloid, fracture, and flow properties.

The snapshots in Fig. 3 qualitatively illustrate plume distributions when the mean colloid displacement is $\overline{M}_1 = 2.5$, 5.0, 7.5, and 10.0 m from the release point subject to three different gravity angles of −75°, 0°, and 75°. Note that the fracture was extended to infinite length to allow snapshots out to mean colloid travel distances of 10 m (this yields a more illustrative figure). Plume constituents are colored according to their size with the smallest third red, middle third green, and largest third blue.[1] Clearly, the smallest colloids are minimally impacted by gravity and are disperse fairly uniformly across the fracture. The mid-sized colloids show increased gravitational settling and tend toward the bottom of the fracture where the parabolic velocity profile is slower; thus they travel more slowly. The largest colloids (blue) are most slowed because gravity keeps them near the fracture bottom where the velocity is slowest. In fact, the largest colloids of the plume are visually distinct as they remain proximate to the fracture wall (note the blue "curves," which are the large colloids one radius distant from the wall, those further from the wall are larger). Moreover, at an angle of 0°, maximum size separation (hydrodynamic chromatography) is observed. At ±75°, less size separation is observed, but at 75° the colloids are gravity assisted (from left to right) as observed by comparing the slowest moving colloids (blue) in the bottom panels of the leftmost and rightmost figures. Variations of the gravity vector in relation to the fracture flow direction are evident for the largest (blue) colloids; they are most impacted and either slowed against the flow direction (Fig. 3, left column) or assisted (Fig. 3, right column).

For the fracture examined in this work, the first normalized spatial moment, $\overline{M}_1$, is always 8 m. Furthermore, the zeroth spatial and temporal moments for the plumes (colloid masses) are 5.24×10^{-15}, 9.92×10^{-15}, 1.61×10^{-14}, and 1.74×10^{-14} m^{-3} (multiply by the colloid density to get mass) for $\sigma_{d_p} = 0$, 0.6, 1.2, and 1.8 μm, respectively.

Fig. 4 shows results for the monodisperse colloid plume; m_1 (see top set of curves) is the time when the first spatial moment is 8 m, the average residence time in an 8-m fracture. The m_1 curves show that as colloid density increases, the time to travel 8 m increases because gravity "sinks" more of the colloids toward the bottom of the fracture where velocities are slow (the same effect would be observed if the colloids were less dense than water and "float"). Colloids are slowest at angles near zero because gravity acts to more directly sink them toward the bottom of the fracture. Finally, the curves are not symmetric because for negative angles, gravity acts against colloid transport down the fracture whereas positive angles assist colloids in the flow direction. Spread (or dispersion, $\overline{M}_2$, in Fig. 4) is increased for less dense colloids because they are better able to sample the entire velocity distribution and experience hydrodynamic dispersion. Also, these effects are most pronounced at large angles because, once again, colloids are better able to sample the entire velocity distribution. These results show the most effect of noise due to the nature of the particle

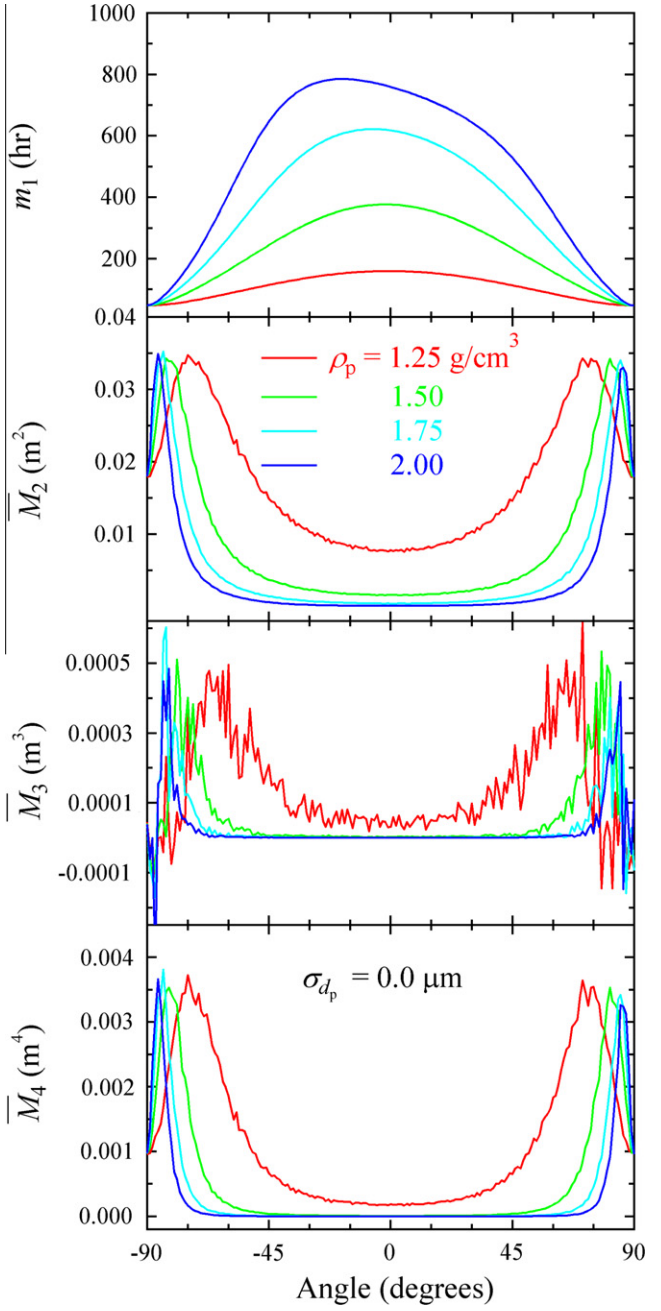

Fig. 4. First absolute temporal and second through fourth normalized spatial moments for monodisperse colloids ($d_p = 1$ μm, $\sigma_{d_p} = 0.0$ μm) where curve colors indicate colloid density.

tracking algorithm. Increasing the number of colloids in the analysis would smooth the results. Little skewness, $\overline{M}_3$, is observed for near-zero angles because these plumes are monodisperse and each constituent is equally affected by gravity (i.e., Brownian motion acting equally in each direction keeps colloids normally distributed). Skewness increases for large angles (positive and negative) because of the increased impacts of hydrodynamic dispersion (especially for less-dense colloids) because they are more uniformly distributed across the fracture and colloids near the center travel fastest because velocity is highest there. This effect is increasingly diminished for more-dense colloids as deviation from ±90° increases. Overall, kurtosis, $\overline{M}_4$, is essentially zero (as is the skewness) because the y-axis scale spans only a short range. This means that the colloid distribution is quite flat and only less so

[1] For interpretation of colour in Figs. 3–6, the reader is referred to the web version of this article.

at large-magnitude angles for low-density colloids. Results for monodisperse colloids in Fig. 4 are quite different from those of polydisperse colloids.

The first absolute temporal moments (residence times) are shown for polydisperse colloids in Fig. 5. In each case, more-dense colloids take longer to travel 8 m with maximum travel times near 0° (actually slightly less than 0° because gravity works against colloid transport down the fracture for negative angles). Increasing the dispersity of the colloid plume, σ_{d_p}, tends to increase the speed with which the plume travels down the fracture because there are more smaller colloids, which are less impacted by gravity and more likely to sample the entire parabolic velocity distribution and travel close to the mean flow speed. All curves are tilted slightly to the right demonstrating how gravity works against the flow direction for negative angles.

Second (top row), third (middle row), and fourth (bottom row) spatial normalized moments obtained at the instant when the center of the plumes have traveled 8 m from the inlet are shown for polydisperse colloid plumes in Fig. 6 (with polydispersity increasing across the columns). In all cases, increased colloid density increases these magnitudes. Also, angles closer to zero increase spatial moment magnitudes because gravity directs colloids directly to the bottom of the fracture where flow speeds are slowest. As colloid polydispersity increases, there are more smaller colloids in the plume and these are less impacted by gravity – hence decreased impacts on spatial moments due to gravity. Careful examination of the results presented in Fig. 6 reveals that for horizontal or near horizontal flow, where the angle is approximately 0° and gravity sinks colloids to the bottom of the fracture, colloids spread the most. This is in agreement with the results presented in the

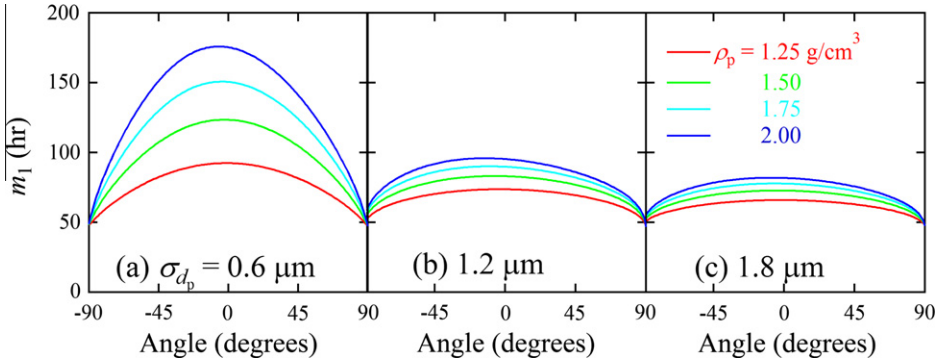

Fig. 5. First absolute temporal moments of the three polydisperse plumes and four colloid densities.

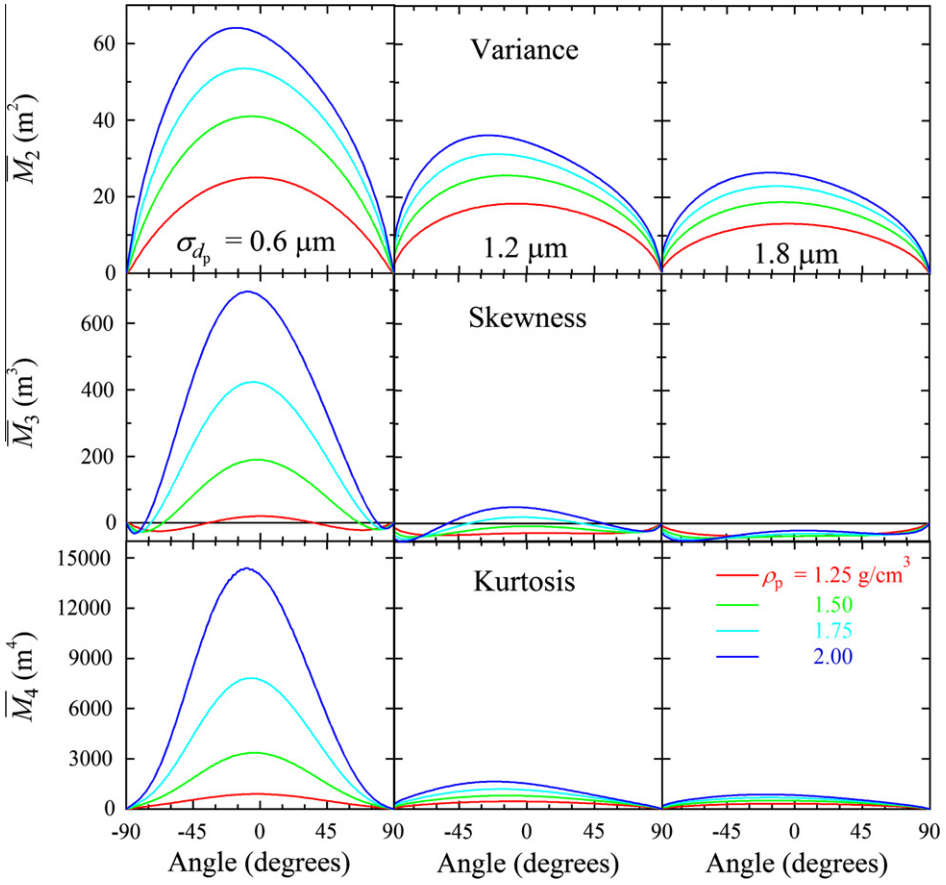

Fig. 6. Second, third, and fourth spatial normalized moments for three polydisperse colloid plumes and four colloid densities.

middle column of Fig. 3, where the mid-sized green colloids are more visible. Furthermore, for horizontal flow conditions colloids are skewed the most. Note that the smallest colloids are least impacted by gravity and travel near the mean flow velocity while the large constituents sink and travel very slowly. Again, this observation is in agreement with the results presented in the middle column of Fig. 3. Also, the plume is leptokurtotic as the flow angle is closest to 0° (the plume has increased colloid concentrations closer to the center of the distribution even if the distribution is widest and has a high second spatial moment).

4. Conclusions

A constant-spatial-step particle tracking numerical model was developed to investigate colloid transport in a one-dimensional, water-saturated fracture with uniform aperture. The fracture was rotated through 180° to capture the effects of gravity on monodisperse as well as polydisperse colloid plumes. It was found that fracture angle, or equivalently the angle of gravity with respect to the fracture flow direction, significantly impacted the migration behavior of colloids within the fracture. The spreading, skewness, and kurtosis of the plume distributions were most pronounced at horizontal or near horizontal flow conditions where the smallest colloids traveled near the mean flow velocity and large colloids sunk and traveled slowly. Increasing the dispersity of the colloids increased the plume movement in the fracture because there were more smaller colloids, which were less affected by gravity and more likely to sampled the entire parabolic velocity profile. Moreover, polydispersity also impacted the shape characteristics of the plume, especially in conjunction with gravitational effects because gravity affected larger colloids more than smaller colloids. Another point to make was that the large colloids sunk faster and had decreased Brownian motion. Finally, the second through fourth spatial moments and the first temporal moment were estimated as functions of fracture orientation angle and colloid density. It was important to recognize that in all cases, larger particles tended to spread over wider sections of the fracture in the flow direction, but smaller particles could travel faster or slower than larger particles depending on fracture orientation angle.

Acknowledgement

Sandia National Laboratories is a multi-program laboratory managed and operated by Sandia Corporation, a wholly owned subsidiary of Lockheed Martin Corporation, for the US Department of Energy's National Nuclear Security Administration under contract DE-AC04-94AL85000.

References

[1] McCarthy JF, Degueldre C. In: Buffle J, van Leeuwen HP, editors. Environmental particles. Lewis, Boca Raton, FL, 1993. p. 247 [Chapter 6].
[2] Singurindy O, Berkowitz B. The role of fractures on coupled dissolution and precipitation patterns in carbonate rocks. Adv Water Res 2005;28:507–21.
[3] Masciopinto C, La Mantia R, Chrysikopoulos CV. Fate and transport of pathogens in a fractured aquifer in the Salento area, Italy. Water Res Res 2008;44:W01404.
[4] Chrysikopoulos CV, Masciopinto C, La Mantia R, Manariotis ID. Removal of biocolloids suspended in reclaimed wastewater by injection in a fractured aquifer model. Environ Sci Technol 2010;44:971–7.
[5] Smith PA, Degueldre C. Colloid-facilitated transport of radionuclides through fractured media. J Contam Hydrol 1993;13:143–66.
[6] Mills WB, Liu S, Fong FK. Literature review and model (COMET) for colloid/metals transport in porous media. J Contam Hydrol 1991;52:213–44.
[7] Abdel-Salam A, Chrysikopoulos CV. Modeling of colloid and colloid-facilitated contaminant transport in a 2-dimensional fracture with spatially-variable aperture. Transp Porous Media 1995:197–221.
[8] Abdel-Salam A, Chrysikopoulos CV. Analysis of a model for contaminant transport in fractured media in the presence of colloids. J Hydrol 1995;165:261–81.
[9] van der Lee J, Ledoux E, de Marsily H. Modeling of colloidal uranium transport in a fractured medium. J Hydrol 1992;139:135–58.
[10] Oswald JG, Ibaraki M. Migration of colloids in discretely fractured porous media: effect of colloidal matrix diffusion. J Contam Hydrol 2001;52:213–44.
[11] Liu HH, Bodvarrson GS, Pan L. Determination of particle transfer in random walk particle methods for fractured porous media. Water Res Res 2000;36:707–13.
[12] Ledin A, Karlsson S, Düker A, Allard B. Measurements in-situ of concentration and size distribution of colloidal matter in deep groundwater by photon correlation spectroscopy. Water Res 1994;28:1539–45.
[13] James SC, Chrysikopoulos CV. Transport of polydisperse colloids in a saturated fracture with spatially variable aperture. Water Resour Res 2000;36:1457–65.
[14] James SC, Chrysikopoulos CV. Transport of polydisperse colloid suspensions in a single fracture. Water Resour Res 1999;35:707–18.
[15] Abdel-Salam A, Chrysikopoulos CV. Unsaturated flow in a quasi-three-dimensional fractured medium with spatially variable aperture. Water Resour Res 1996;32:1531–40.
[16] James SC, Chrysikopoulos CV. Analytical solutions for monodisperse and polydisperse colloid transport in uniform fractures. Colloids Surf A – Physicochem Eng Aspects 2003;226:101–18.
[17] de Marsily G. Quantitative hydrogeology: groundwater hydrology for engineers. San Diego, California: Academic Press, Inc; 1986.
[18] Abdel-Salam A, Chrysikopoulos CV. Analytical solutions for one-dimensional colloid transport in saturated fractures. Adv Water Resour 1994;17:283–96.
[19] Hwang Y, Chanber PL, Lee WW-L. TH Pigford. Analytic studies of colloid transport in fractured porous media. Berkeley, CA: Lawrence Berkeley National Laboratory; 1989.
[20] Tien NC, Jen CP. Analytical modeling for colloid-facilitated transport of *n*-member radionuclides chain in the fractured rock. Nucl Sci Technol 2007;18:336–43.
[21] Chrysikopoulos CV, Abdel-Salam A. Modeling colloid transport and deposition in saturated fractures. Colloids Surf A – Physicochem Eng Aspects 1997;121:189–202.
[22] Ibaraki M, Sudicky EA. Colloid-facilitated contaminant transport in discretely fractured porous media. 1. Numerical formulation and sensitivity analysis. Water Resour Res 1995;31:2945–60.
[23] Reimus PW. The use of synthetic colloids in tracer transport experiments in saturated rock fractures. Los Alamos: Los Alamos National Laboratory; 1995.
[24] Grindrod P, Lee AJ. Colloid migration in symmetrical non-uniform fractures: particle tracking in three dimensions. J Contam Hydrol 1997;27:157–75.
[25] Chrysikopoulos CV, James SC. Transport of neutrally buoyant and dense variably sized colloids in a two-dimensional fracture with anisotropic aperture. Transp Porous Media 2003;51:191–210.
[26] James SC, Chrysikopoulos CV. Dense colloid transport in a bifurcating fracture. J Colloid Interface Sci 2004;270:250–4.
[27] James SC, Bilezikjian TK, Chrysikopoulos CV. Contaminant transport in a fracture with spatially variable aperture in the presence of monodisperse and polydisperse colloids. Stochastic Environ Res Risk Assess 2005;19:266–79.
[28] Reno MD, James SC, Altman SJ. Colloid dispersion in a uniform-aperture fracture. J Colloid Interface Sci 2006;300:383–90.
[29] Tompson AFB, Gelhar LW. Numerical simulation of solute transport in three-dimensional, randomly heterogeneous porous media. Water Resour Res 1990;36:2541–62.
[30] James SC, Chrysikopoulos CV. An efficient particle tracking equation with specified spatial step for the solution of the diffusion equation. Chem Eng Sci 2001;56:6535–43.
[31] Reimus PW, James SC. Determining the random time step in a constant spatial step particle tracking algorithm. Chem Eng Sci 2002;57:4429–34.
[32] Russel WB, Saville DA, Schowalter WR. Colloidal dispersions. Cambridge, UK: Cambridge University Press; 1989.
[33] Ang AH-S, Tang WH. Probability concepts in engineering planning and design. Basic principles, 1. New York, NY: Wiley and Sons; 1975.
[34] Haas CN. Moment analysis of tracer experiments. J Environ Eng ASCE 1996;122.
[35] Aris R. On the dispersion of a solute in a fluid flowing through a tube. Proc Roy Soc Lond A 1956;235:67–77.
[36] Brenner H. Dispersion resulting from flow through spatially periodic porous media. Philos Trans Roy Soc Lond A 1980;297:81–133.
[37] Goltz M, Roberts PV. Using the method of moments to analyze 3-dimensional diffusion-limited solute transport from temporal and spatial perspectives. Water Resour Res 1987;23:1575–85.
[38] Valocchi AJ. Spatial moment analysis of the transport of kinetically adsorbing solutes through stratified aquifers. Water Resour Res 1989;25:273–9.
[39] Chrysikopoulos CV, Kitanidis PK, Roberts PV. Macrodispersion of sorbing solutes in heterogeneous porous formations with spatially periodic retardation factor and velocity field. Water Resour Res 1992;28:1517–29.
[40] Chrysikopoulos CV, Kitanidis PK, Roberts PV. Generalized Taylor–Aris moment analysis of the transport of sorbing solutes through porous media with spatially-periodic retardation factor. Trans Porous Media 1992;7:163–85.